PERGAMON

International Journal of Solids and Structures 39 (2002) 1757–1775

INTERNATIONAL JOURNAL OF SOLIDS and STRUCTURES

www.elsevier.com/locate/ijsolstr

Effect of *T*-stress and loading rate on crack initiation in rate sensitive plastic materials

K.R. Jayadevan [b], R. Narasimhan [a,*], T.S. Ramamurthy [b], B. Dattaguru [b]

[a] *Department of Mechanical Engineering, Indian Institute of Science, Bangalore 560 012, India*
[b] *Department of Aerospace Engineering, Indian Institute of Science, Bangalore 560 012, India*

Received 21 August 2001; received in revised form 19 November 2001

Abstract

The objectives of this paper are to examine the validity of a two-parameter (J–Q) characterization of quasi-static crack tip fields in rate sensitive plastic solids and, also to investigate the influence of strain rate sensitivity of the material on the variation of fracture toughness with loading rate. To this end, 2D plane strain finite element analyses of a boundary layer model loaded quasi-statically and a single edge notched (tensile) specimen under dynamic loading are performed. The material is assumed to obey a J_2 viscoplasticity model and a small strain formulation is employed. The results demonstrate that a valid J–Q field exists in low to moderately rate sensitive materials under quasi-static loading (i.e., when inertial effects are neglected). The opposing effects of strain rate sensitivity and material inertia are reflected in the stress field ahead of the tip in the dynamically loaded specimen. The variation of fracture toughness K_{dc} with loading rate $\dot{K}$ for cleavage cracking is predicted using a simple critical stress criterion. It is found that strain rate sensitivity index of the material has a profound effect on the K_{dc}–$\dot{K}$ variation.

Keywords: Rate dependent plastic solids; J–Q field; Loading rate; Finite elements; Cleavage fracture; Dynamic fracture toughness

1. Introduction

A precise understanding of the influence of material inertia and strain rate sensitivity on crack initiation is of vital importance while designing structural components to resist dynamic fracture (Rosakis and Ravichandran, 2000). Some examples of such applications are blast loading in an aircraft, pressure vessels subjected to shock loading, etc. (Kanninen and O'Donoghue, 1995).

The dynamic fracture toughness K_{dc} for many engineering materials depends strongly on the stress intensity rate $\dot{K}$. Several experimental investigations (Ravi-Chandar and Knauss, 1984; Dally and Barker, 1988; Zehnder and Rosakis, 1990; Owen et al., 1998a,b; Venkert et al., 1998) have shown that a steep elevation in K_{dc} occurs at high loading rates. By contrast, it has been found in certain materials (Priest,

* Corresponding author. Tel.: +91-80-394-2959; fax: +91-80-360-0648.
E-mail address: narasi@mecheng.iisc.ernet.in (R. Narasimhan).

0020-7683/02/$ - see front matter
PII: S0020-7683(02)00012-4

1976) that K_{dc} decreases as $\dot{K}$ increases within a nominal range (1–10^4 MPa $\sqrt{m}$/s). This observation was further supported by many other studies (see, for example, Costin and Duffy, 1979; Klepaczko, 1982; Kalthoff, 1986). These contrasting trends in the K_{dc}–$\dot{K}$ behaviour are generally rationalized based on the failure mechanisms (Freund, 1990). Thus, strain rate sensitive materials which fail by a cleavage mechanism are expected to show a lower K_{dc} compared to the static fracture toughness K_c, whereas the reverse trend is suggested for materials which fail by a ductile void coalescence mechanism. However, these arguments have not taken into account the effect of material inertia on the stress field or void growth rate near the crack tip. In this context, it must be mentioned that Basu and Narasimhan (2000) have recently shown that the stress field ahead of the tip in a rate independent elastic–plastic solid decreases as loading rate increases. Thus, material inertia may oppose the role of strain rate sensitivity during dynamic crack initiation. Hence, a systematic investigation of these two factors on stress fields and plastic zone near the crack tip and variation of K_{dc} with $\dot{K}$, particularly for the cleavage mode of failure, needs to be undertaken. This is important because a decrease in K_{dc} as $\dot{K}$ increases, raises the risk of fracture when such materials are subjected to dynamic loading.

The investigations of Koppenhoefer and Dodds (1996) and Basu and Narasimhan (2000) have shown that crack tip constraint or triaxiality may be reduced under dynamic loading. In this context, it must be mentioned that the limitation of a one-parameter characterization of quasi-static elastic–plastic crack tip fields based on J-integral (Hutchinson, 1968; Rice and Rosengren, 1968) is well recognized (Al-Ani and Hancock, 1991; O'Dowd and Shih, 1991). Hence, approaches based on J (or K) and a triaxiality parameter Q (O'Dowd and Shih, 1991, 1992) or, equivalently T-stress under quasi-static, small scale yielding conditions (Betegón and Hancock, 1991) have been proposed. Basu and Narasimhan (2000) observed that a fracture geometry which shows no constraint loss under static loading can exhibit strong negative Q when loaded dynamically. Since Q and T are related under static loading (see O'Dowd and Shih, 1992), the above observation motivated Jayadevan et al. (2001a) to conduct a systematic study of the evolution of T-stress in dynamically loaded linear elastic fracture specimens. Their results demonstrated that the biaxiality parameter $\beta = T\sqrt{\pi a}/K$, where a is the crack length, is strongly negative during the early stages of dynamic loading as compared to the static limit, which corroborates well with the analytical work of Liu et al. (1998).

Jayadevan et al. (2001b) demonstrated that a valid J–Q field exists under dynamic loading irrespective of the specimen geometry and loading rate in rate independent plastic solids. Further, it was shown that the strong negative Q observed at high $\dot{K}$ correlates well with the large negative T in the corresponding elastic analyses (Jayadevan et al., 2001a) and contributes to the elevation in K_{dc} at high loading rates. However, as mentioned earlier, such an investigation for strain rate sensitive plastic solids has not been undertaken. In this context, it must be noted that the effect of T-stress on the quasi-static crack tip fields for such solids has also not been addressed. Here, an important issue is the absence of a proper reference solution (such as the HRR solution for the rate independent case) which can be used as the basis for defining constraint loss.

Thus, the objectives of the present paper are as follows. First, the validity of the two-parameter (J–Q) characterization of quasi-static crack tip fields will be systematically assessed. The effect of T-stress on the Q-term as well as near-tip plastic zone for different strain rate sensitivity indices (m) and loading rates will be examined. Secondly, the effect of loading rate on the stress field ahead of the tip and plastic zone in a dynamically loaded fracture specimen will be investigated for different values of m. The correlation between these results and the T-stress histories obtained by Jayadevan et al. (2001a) in their linear elastic analyses will be studied. Finally, the variation of K_{dc} with $\dot{K}$ will be predicted using a simple critical stress criterion and the influence of m on this variation will be investigated.

To this end, 2D plane strain, quasi-static boundary layer analyses as well as quasi-static and dynamic finite element analyses of a single edge notched specimen under tensile loading (SEN(T)) are performed. In the quasi-static analyses, time dependent loading is applied but inertial effects are neglected. The material is assumed to obey a J_2 viscoplasticity model and a small strain formulation is employed. The stress field

ahead of the crack tip and the near-tip plastic zones are examined in both sets of analyses. A critical stress criterion (Ritchie et al., 1973) is employed to predict cleavage crack initiation from the analyses of the fracture specimen. The results show that a two-parameter characterization of quasi-static crack tip field is possible in low and moderately rate sensitive plastic materials. Further, it is found that the strain rate sensitivity index of the material profoundly affects the stress distribution ahead of the tip in the dynamically loaded specimen as well as the variation of fracture toughness with loading rate.

2. Modified boundary layer analyses

In this section, modified boundary layer analyses are conducted for rate sensitive materials under mode I, plane strain conditions. The stress distribution ahead of the crack tip and the plastic zone corresponding to different values of rate sensitivity, loading rate and T-stress levels are studied.

2.1. Modelling aspects

A semi-circular domain containing a crack is considered as shown in Fig. 1. The displacement components based on the first and second terms of the elastic mode I, plane strain crack tip field (Williams, 1957), which are characterized by the stress intensity factor K and the T-stress, respectively, are prescribed on the outer boundary of this domain. By linearly varying this remote K–T field with time, static equilibrium solutions corresponding to different (constant) stress intensity rates $\dot{K}$ are obtained. Hence, inertial effects are not considered in this model. As shown in Fig. 1, mode I symmetry conditions are applied along the line ahead of the crack tip ($\theta = 0$), while traction-free conditions are enforced on the crack line ($\theta = 180°$).

The material is assumed to obey the viscoplastic constitutive model proposed by Peirce et al. (1984), in which the effective viscoplastic strain rate $\dot{\bar{\varepsilon}}^{\mathrm{p}}$ is taken to be given by,

$$\dot{\bar{\varepsilon}}^{\mathrm{p}} = \dot{\varepsilon}_0 \left(\frac{\bar{\sigma}}{g(\bar{\varepsilon}^{\mathrm{p}})} \right)^{1/m}. \tag{1}$$

Here, m is a strain rate exponent, $\dot{\varepsilon}_0$ is a reference strain rate and $g(\bar{\varepsilon}^{\mathrm{p}})$ is a strain hardening function. It should be noted that rate independent behaviour will be obtained as $m \to 0$. Further, the effective stress $\bar{\sigma} = (3/2 S_{ij} S_{ij})^{1/2}$, where S_{ij} is the deviatoric stress and the equivalent plastic strain $\bar{\varepsilon}^{\mathrm{p}} = \int_0^t (2/3 \dot{\varepsilon}^{\mathrm{p}}_{ij} \dot{\varepsilon}^{\mathrm{p}}_{ij})^{1/2} \mathrm{d}t$, where $\dot{\varepsilon}^{\mathrm{p}}_{ij}$ is the viscoplastic part of the strain rate tensor. The function $g(\bar{\varepsilon}^{\mathrm{p}})$ is chosen to represent an isotropic power law hardening material with a strain hardening exponent n such that

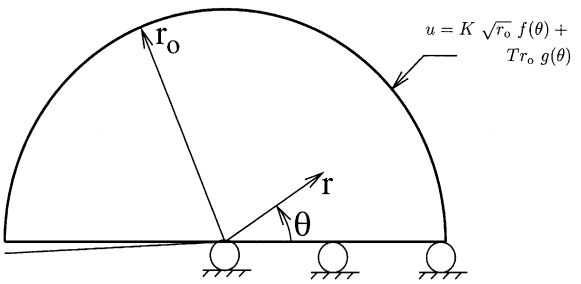

Fig. 1. Schematic of the modified boundary layer model showing boundary conditions.

$$g(\bar{\varepsilon}^{\mathrm{p}}) = \sigma_0 \left(\frac{\bar{\varepsilon}^{\mathrm{p}}}{\varepsilon_0} + 1 \right)^{1/n} . \tag{2}$$

Here, σ_0 and $\varepsilon_0 = \sigma_0/E$ are the initial yield stress and strain. The Young's modulus E, Poisson's ratio ν, initial yield stress σ_0, strain hardening exponent n and reference strain rate $\dot{\varepsilon}_0$ are chosen as 200 GPa, 0.3, 400 MPa, 10 and 0.1 s^{-1}, respectively. Three values of m (viz., 0.004, 0.02 and 0.1) are used to examine the rate sensitivity effects. The generalization of Eq. (1) to multiaxial states is accomplished by employing the Von Mises model (see Peirce et al., 1984).

The rate tangent modulus method proposed by Peirce et al. (1984) is employed to implement the elastic–viscoplastic constitutive model in a small strain finite element procedure. A small time step size (less than $0.01(\varepsilon_0/\dot{\varepsilon}_0)$) is used in the analyses as suggested by Peirce et al. (1984) so that the numerical solution remains stable. The B-bar method proposed by Hughes (1980) is employed to alleviate the over-stiff response exhibited by the finite element solution due to plastic incompressibility.

The finite element mesh used to represent the semi-circular domain shown in Fig. 1 is composed of four-noded isoparametric quadrilateral elements and is well refined near the crack tip. The size of the smallest element near the crack tip is 10^{-6} times the radius r_0 of the outer boundary of the domain. The analyses are carried out for different stress intensity rates $\dot{K}$ ranging from 10^5 to 10^7 MPa $\sqrt{\mathrm{m}}$/s, by incrementing the remote K–T field linearly with time while holding the ratio T/K fixed. Further, in all the analyses, the maximum size of the plastic zone is maintained within $r_0/20$ so that the boundary layer formulation remains valid.

2.2. Results and discussion

It has been shown by O'Dowd and Shih (1991, 1992) that the near-tip stress and strain fields in rate independent plastic solids can be adequately characterized by J and the triaxiality parameter Q. In other words, at a given level of Q (or, equivalently, T under small scale yielding conditions), the stresses and strains ahead of the tip remain self-similar when plotted against $r\sigma_0/J$. However, in a rate sensitive plastic solid, an additional dependence of the near-tip fields on $\dot{J}$ (or, $\dot{K}$ under small scale yielding conditions) is expected.

2.2.1. Structure of crack tip fields

Dimensional considerations show that the near-tip fields in a rate sensitive plastic solid under quasi-static, small scale yielding conditions are expected to have the following form, when K and T increase proportionally:

$$\frac{\sigma_{ij}}{\sigma_0} = \tilde{\sigma}_{ij}\left(\frac{r\sigma_0}{J}, \theta; \frac{\dot{K}}{K\dot{\varepsilon}_0}, \frac{T}{\sigma_0}, m, \frac{E}{\sigma_0}, n \right), \tag{3}$$

$$\frac{\varepsilon^{\mathrm{p}}_{ij}}{\varepsilon_0} = \tilde{\varepsilon}_{ij}\left(\frac{r\sigma_0}{J}, \theta; \frac{\dot{K}}{K\dot{\varepsilon}_0}, \frac{T}{\sigma_0}, m, \frac{E}{\sigma_0}, n \right). \tag{4}$$

Unlike in rate independent materials (Betegón and Hancock, 1991), the above functional relationships involve two additional terms (viz., $\dot{K}/K\dot{\varepsilon}_0$ and m). This implies that for a given T/σ_0 and material properties, $\dot{K}/K\dot{\varepsilon}_0$ parametrizes the family of near-tip fields when the radial distance r from the crack tip is normalized by J/σ_0.

In order to verify the self-similar nature of the fields for a given value of $\dot{K}/K\dot{\varepsilon}_0$, T/σ_0 and material properties, the results obtained from a set of quasi-static, small scale yielding analyses are presented in

Fig. 2(a)–(d). In Fig. 2(a), the variations of σ_{11}/σ_0 with $r\sigma_0/J$ ahead of the tip are plotted for different sets of $\dot{K}$ and K, but at a fixed ratio of $\dot{K}/K\dot{\varepsilon}_0 = 4 \times 10^5$. These results correspond to $T = 0$ and $m = 0.1$. Similar variations of σ_{22}/σ_0, equivalent plastic strain $\bar{\varepsilon}^p/\varepsilon_0$ and its rate $\dot{\bar{\varepsilon}}^p/\dot{\varepsilon}_0$ are shown in Fig. 2(b)–(d), respectively. It can be seen from these results that at a given $\dot{K}/K\dot{\varepsilon}_0$, the near-tip fields when plotted against $r\sigma_0/J$ remain invariant. In other words, the near-tip fields in rate sensitive plastic materials under small scale yielding conditions are not independent of K when plotted against $r\sigma_0/J$ for any given $\dot{K}$. Hence, all the results from the boundary layer analyses will be presented below corresponding to a fixed value of $K = 50$ MPa $\sqrt{\text{m}}$. This magnitude of K is chosen to facilitate comparison of some of these results with those from the specimen analyses (see Section 3).

2.2.2. Stress distributions ahead of the crack tip

In Fig. 3(a) and (b), the variations of normalized opening stress σ_{22}/σ_0 with normalized radial distance $r\sigma_0/J$ ahead of the tip are shown for $m = 0.004$ and 0.1, respectively. These figures pertain to $T = 0$. Results corresponding to different $\dot{K}$ and a fixed $K = 50$ MPa $\sqrt{\text{m}}$ are presented in each of the above figures.

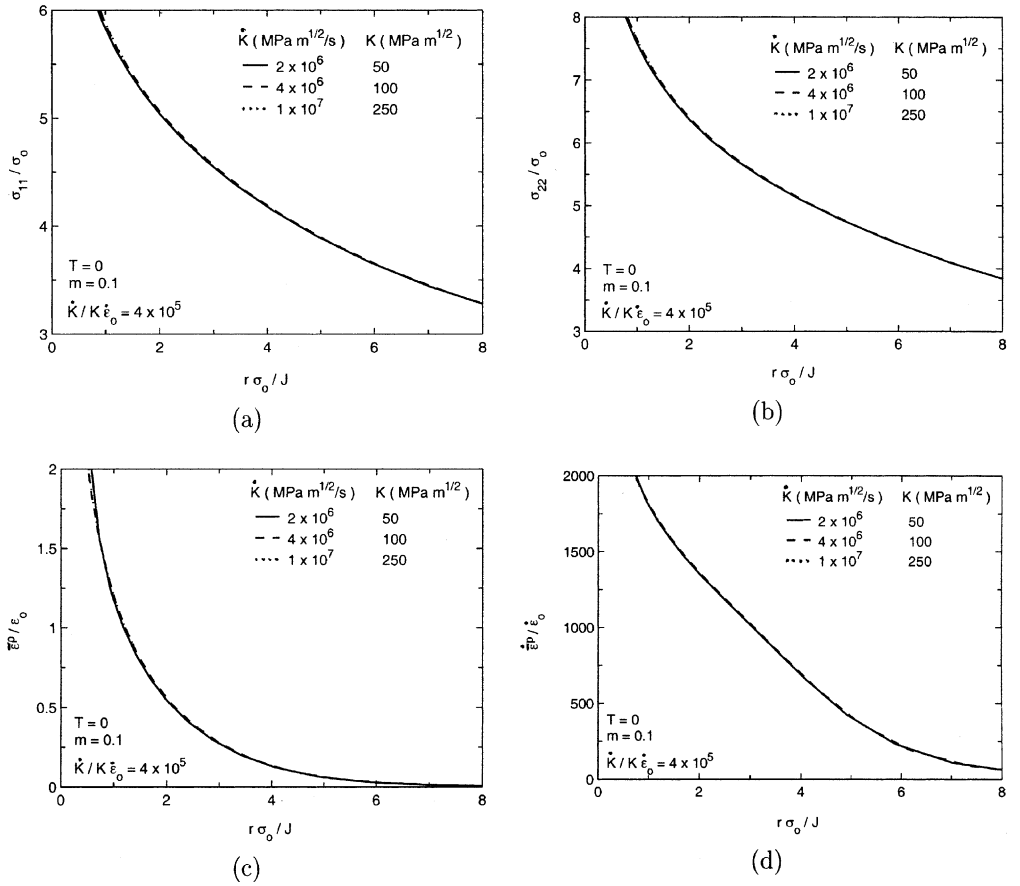

Fig. 2. The variations of (a) σ_{11}/σ_0, (b) σ_{22}/σ_0, (c) $\bar{\varepsilon}^p/\varepsilon_0$ and (d) $\dot{\bar{\varepsilon}}^p/\dot{\varepsilon}_0$ with normalized radial distance ahead of the crack tip obtained from the boundary layer analyses for different values of $\dot{K}$ and K, but corresponding to fixed values of $\dot{K}/K\dot{\varepsilon}_0 = 4 \times 10^5$, $T = 0$ and $m = 0.1$.

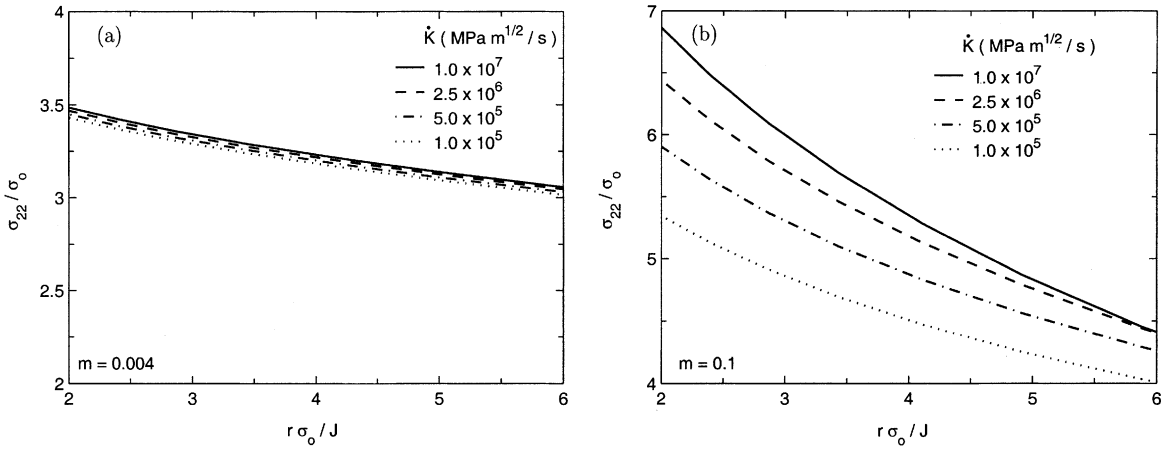

Fig. 3. The variation of σ_{22}/σ_0 ahead of the crack tip with normalized radial distance obtained from the boundary layer analyses with $T = 0$ corresponding to different loading rates and fixed $K = 50$ MPa $\sqrt{\text{m}}$ for (a) $m = 0.004$ and (b) $m = 0.1$.

It may be noted from Fig. 3(a) that corresponding to a low value of m, the effect of loading rate on the opening stress ahead of the crack tip is marginal. Thus, for example, σ_{22}/σ_0 at a normalized radial distance of $r\sigma_0/J = 4$ corresponding to $m = 0.004$ increases by about 1.5% when the loading rate $\dot{K}$ is increased from 10^5 to 10^7 MPa $\sqrt{\text{m}}$/s. Also, the variation of σ_{22}/σ_0 corresponding to $m = 0.004$ and $\dot{K} = 10^5$ MPa $\sqrt{\text{m}}$/s is only slightly higher (by less than 2%) than that for the rate independent case obtained by Jayadevan et al. (2001b). By contrast, σ_{22} increases significantly with loading rate for a highly rate sensitive material (see Fig. 3(b)). Further, this enhancement is more pronounced very near the crack tip which is not surprising because $\dot{\bar{\varepsilon}}^p$ is large near the tip. For example, σ_{22}/σ_0 at $r\sigma_0/J = 4$ in Fig. 3(b) increases by about 19% as $\dot{K}$ enhances from 10^5 to 10^7 MPa $\sqrt{\text{m}}$/s. Here, it must be noted that although an increase in $\dot{K}$ of two orders of magnitude is considered above, the plastic strain rate near the tip does not increase by the same ratio.

In Fig. 4(a) and (b), the radial variation of normalized opening stress ahead of the tip for the case $m = 0.02$ are displayed corresponding to $\dot{K} = 10^5$ and 10^7 MPa $\sqrt{\text{m}}$/s, respectively. In each of the above

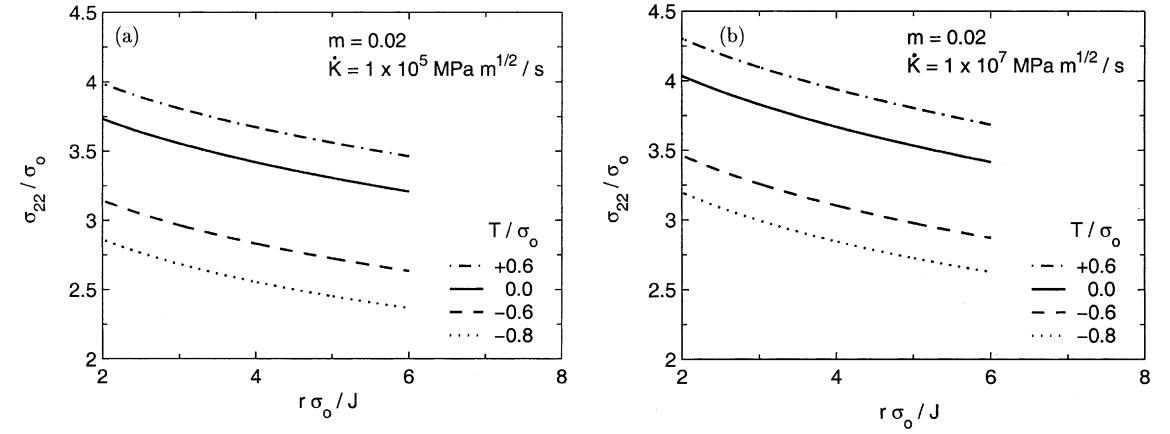

Fig. 4. The variation of normalized opening stress with radial distance ahead of the crack tip obtained from the boundary layer analyses for different T-stress values and corresponding to loading rates, $\dot{K}$, of (a) 10^5 and (b) 10^7 MPa $\sqrt{\text{m}}$/s for a material with $m = 0.02$. All results pertain to $K = 50$ MPa $\sqrt{\text{m}}$.

figures, results pertaining to different values of T/σ_0 are presented. It may be seen from Fig. 4(a) and (b) that at a given $\dot{K}$, the opening stress ahead of the tip is significantly lowered when T is negative. On the other hand, there is some elevation in σ_{22} ahead of the tip when T is positive. Also, the family of curves plotted in Fig. 4(a) and (b) pertaining to different levels of T appear parallel to each other. This was found to be true for other values of rate sensitivity index m, as well, except for highly rate sensitive materials at very high $\dot{K}$ (for example, $m = 0.1$ at $\dot{K} = 10^7$ MPa $\sqrt{\text{m}}$/s). All the features discussed above are qualitatively similar to those observed for rate independent materials (O'Dowd and Shih, 1991). Further, on comparing Fig. 4(a) and (b), it can be noticed that σ_{22} at a given $r\sigma_0/J$ increases with $\dot{K}$ irrespective of T-stress. Also, it is found to enhance with m irrespective of T at a given $\dot{K}$.

2.2.3. Difference stress field

The validity of a J–Q characterization of quasi-static crack tip fields in rate dependent materials is examined in this subsection. Jayadevan et al. (2001b) employed the HRR solution as the reference field in defining the difference stresses (i.e., $Q\hat{\sigma}_{ij} = \sigma_{ij} - \sigma_{ij}^{\text{HRR}}$) in their study of constraint effects in rate independent plastic solids under static and dynamic loading. Alternatively, the near-tip solution corresponding to $T = 0$ could have been used as the reference field (see O'Dowd and Shih, 1994). Such an approach was advocated by Koppenhoefer and Dodds (1996) for rate sensitive materials as well. However, it should be noted that the HRR solution or the rate independent solution pertaining to $T = 0$ are not valid reference fields for rate sensitive plastic solids since they do not account for flow stress elevation due to high strain rates. Some modifications to the HRR solution to include strain rate effects have been suggested by Hoff et al. (1985). Recently, Basu and Narasimhan (2000) have also employed a modified HRR solution to examine constraint effects in dynamically loaded rate sensitive fracture specimens. However, these approaches are approximate and are based on ad hoc modification to the rate independent HRR solution. Hence, in this work, the stress variation obtained from the small scale yielding analysis with $T = 0$ corresponding to the respective rate sensitivity index m and $\dot{K}$ is employed as the reference solution in order to compute the difference field under quasi-static loading.

The difference stress field, $Q\hat{\sigma}_{22} = \sigma_{22} - (\sigma_{22})_{T=0}^{\text{SSY}}$, for the case $m = 0.02$ is plotted against $r\sigma_0/J$ in Fig. 5(a) and (b) corresponding to $\dot{K} = 10^5$ and 10^7 MPa $\sqrt{\text{m}}$/s, respectively. Similar radial variations of $Q\hat{\sigma}_{11}$ are shown in Fig. 5(c) and (d). Results pertaining to different levels of T/σ_0 are presented in each of the above figures. It may be observed that positive T-stress gives rise to positive $Q\hat{\sigma}_{22}$ and $Q\hat{\sigma}_{11}$, whereas for negative T, $Q\hat{\sigma}_{22}$ and $Q\hat{\sigma}_{11}$ become significantly negative. Thus, for example, corresponding to $\dot{K} = 10^5$ MPa $\sqrt{\text{m}}$/s, the magnitudes of $Q\hat{\sigma}_{22}$ at $r\sigma_0/J = 4$ are $+0.25$ and -0.59 for $T/\sigma_0 = +0.6$ and -0.6, respectively. The $Q\hat{\sigma}_{22}$ and $Q\hat{\sigma}_{11}$ distributions shown in Fig. 5(a)–(d) vary slowly with distance in the range $2 < r\sigma_0/J < 6$ irrespective of $\dot{K}$. Also, the $Q\hat{\sigma}_{11}$ distributions displayed in Fig. 5(c) and (d) are similar to the $Q\hat{\sigma}_{22}$ variations presented in Fig. 5(a) and (b), which suggests that the difference field is triaxial in nature like in the rate independent case. The above features apply to other values of m as well except for highly rate sensitive materials subjected to very high $\dot{K}$. Finally, it is interesting to note on comparing Fig. 5(a) and (b) or 5(c) and (d) that stress intensity rate $\dot{K}$ has a negligible effect on the difference fields for quasi-static loading.

In order to understand clearly the influence of $\dot{K}$ and m on the features of the difference solution, $Q\hat{\sigma}_{22}$ and the ratio $Q\hat{\sigma}_{22}/Q\hat{\sigma}_{11}$ evaluated at $r\sigma_0/J = 4$, are summarized in Table 1 for different m, $\dot{K}$ and T/σ_0. Also presented in Table 1 is the parameter, Q' defined as $Q' = (Q\hat{\sigma}_{22}|_{r\sigma_0/J=6} - Q\hat{\sigma}_{22}|_{r\sigma_0/J=2})/4$, which indicates how the difference field varies with distance ahead of the tip. The tabulated values of $Q\hat{\sigma}_{22}$ clearly show that it becomes more negative as T-stress increases in the negative sense, irrespective of m and $\dot{K}$. This behaviour is similar to that established by O'Dowd and Shih (1992) for rate independent case. However, the magnitude of $Q\hat{\sigma}_{22}$ decreases as the rate sensitivity index m increases at a particular $\dot{K}$. On the other hand, as already mentioned, the dependence of $Q\hat{\sigma}_{22}$ on $\dot{K}$ is marginal except for the case $m = 0.1$. The values of $Q\hat{\sigma}_{22}/Q\hat{\sigma}_{11}$ for the case $m = 0.004$ and 0.02 are reasonably close to unity and suggest that the difference fields are triaxial in nature. However, these values for $m = 0.1$ are far from unity, particularly at

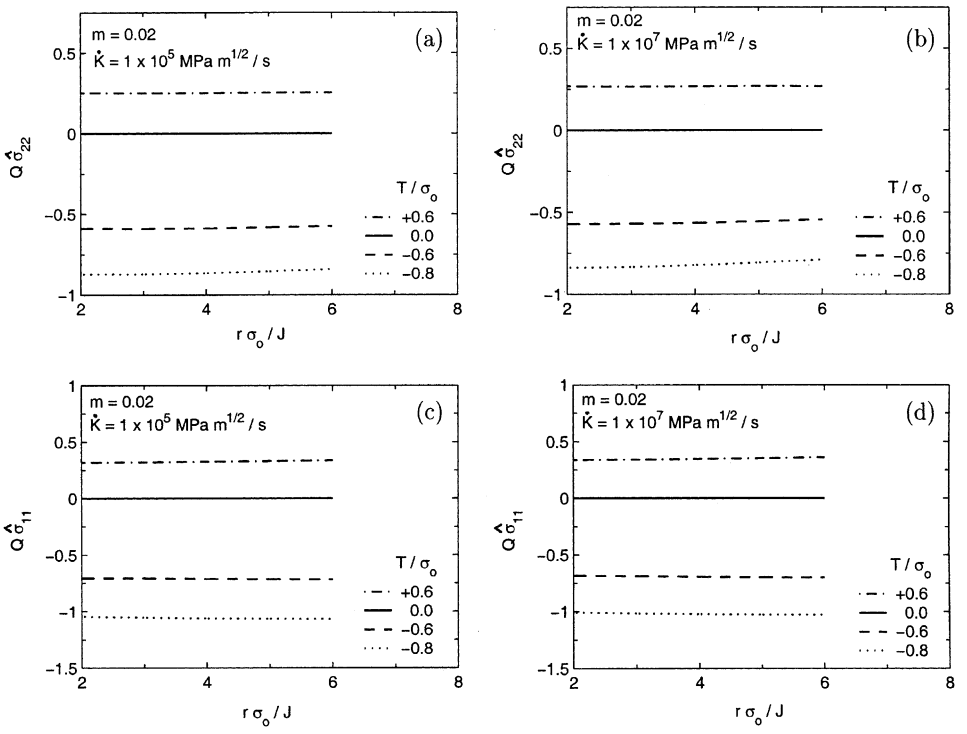

Fig. 5. The variation of difference stress $Q\hat{\sigma}_{22}$ with normalized radial distance ahead of the crack tip obtained from the boundary layer analyses for different T-stress values and corresponding to loading rates, $\dot{K}$, of (a) 10^5 and (b) 10^7 MPa $\sqrt{\text{m}}$/s for a material with $m = 0.02$. Similar results showing the variation of $Q\hat{\sigma}_{11}$ are displayed in (c) and (d). All results pertain to $K = 50$ MPa $\sqrt{\text{m}}$.

Table 1
Values of constraint parameter $Q\hat{\sigma}_{22}$ obtained from the boundary layer analyses corresponding to two values of $\dot{K}$ and T/σ_0 for different rate sensitivity indices. Also indicated are the ratio $Q\hat{\sigma}_{22}/Q\hat{\sigma}_{11}$ and the parameter $|Q'|$. All results pertain to $K = 50$ MPa $\sqrt{\text{m}}$

m	$\dot{K}$ (MPa $\sqrt{\text{m}}$/s)	T/σ_0	$Q\hat{\sigma}_{22}$	$Q\hat{\sigma}_{22}/Q\hat{\sigma}_{11}$	$\lvert Q'\rvert$
0.004	10^5	−0.6	−0.63	0.87	0.01
		−0.8	−0.95	0.86	0.01
	10^7	−0.6	−0.63	0.87	0.00
		−0.8	−0.94	0.86	0.01
0.02	10^5	−0.6	−0.59	0.83	0.00
		−0.8	−0.87	0.82	0.01
	10^7	−0.6	−0.57	0.82	0.01
		−0.8	−0.82	0.80	0.01
0.1	10^5	−0.6	−0.42	0.63	0.02
		−0.8	−0.59	0.62	0.02
	10^7	−0.6	−0.20	0.32	0.07
		−0.8	−0.29	0.34	0.09

$\dot{K} = 10^7$ MPa $\sqrt{\text{m}}$/s. Further, the parameter Q' is quite small in magnitude for $m = 0.004$ and 0.02, whereas, it is around 0.1 for $m = 0.1$ at high $\dot{K}$. Thus, these results confirm that the difference field for low and moderately rate sensitive materials has a structure similar to the rate independent case. On the other hand,

the character of the dominant and second term in the asymptotic solution for the stresses near the tip appears to be strongly influenced by strain rate sensitivity for materials with large m.

2.2.4. Plastic zones

The crack tip plastic zones corresponding to different $\dot{K}$ values for the case $T = 0$ and a highly rate sensitive material with $m = 0.1$ are shown in Fig. 6. It is interesting to note from this figure that the plastic zone is only marginally affected by the loading rate if inertia is neglected (i.e., the analysis is quasi-static). In this connection, it must be mentioned that the levels of $\dot{K}$ considered in Fig. 6 vary by two orders of magnitude. The above key observation applies for other non-zero values of T as well and corroborates with the fact that $\dot{K}$ has negligible influence on the difference stress field under quasi-static loading (see Section 2.2.3). It must also be mentioned that the normalized plastic zone remains invariant with respect to K at any given $\dot{K}$. Thus, the normalized crack tip plastic zone is fairly independent of $\dot{K}/K\dot{\varepsilon}_0$ and depends only on T/σ_0 and material properties.

In order to examine the effect of T-stress on the shape and size of the plastic zone in rate sensitive plastic materials, crack tip plastic zones for different negative T/σ_0 values are displayed in Fig. 7(a) and (b) corresponding to $m = 0.004$ and 0.1, respectively. These figures pertain to a fixed value of $\dot{K} = 10^5$ MPa $\sqrt{\text{m}}$/s. It can be seen from Fig. 7(a) and (b) that with increase in negative T-stress the plastic zone rotates slightly clockwise and increases dramatically in size. This is similar to the observation made by Shih et al. (1993) and Jayadevan et al. (2001b) for rate independent plastic solids. On comparing Fig. 7(a) and (b), it can be seen that the plastic zone for a material with higher m is more upright, less elongated in shape and slightly smaller in size irrespective of T-stress.

Table 2 summarizes the normalized maximum plastic zone size corresponding to different T/σ_0 for two values of m and $\dot{K}$. This table clearly shows the significant increase in size of the plastic zone with negative T-stress irrespective of the value of m and $\dot{K}$. Further, it can be seen that the plastic zone size is unaffected by loading rate at any given T/σ_0. However, for a given loading rate, it marginally decreases with increase in m, which correlates with the decrease in $|Q\hat{\sigma}_{22}|$ with m noted in section 2.2.3.

The boundary layer formulation is not suitable for investigating the effect of stress wave loading on crack initiation. Hence, a finite width geometry (viz., SEN(T)) is considered in the next Section. The results from the quasi-static boundary layer analyses obtained here will be compared in the next section with those from the dynamic analyses of the SEN(T) specimen.

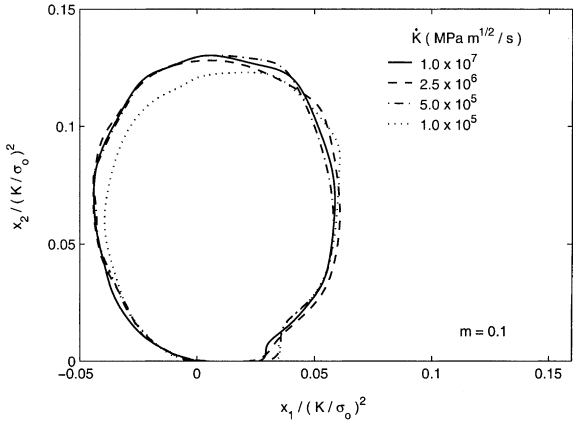

Fig. 6. Crack tip plastic zones obtained from the boundary layer analyses with $T = 0$ corresponding to different loading rates for a material with $m = 0.1$. All results pertain to $K = 50$ MPa $\sqrt{\text{m}}$.

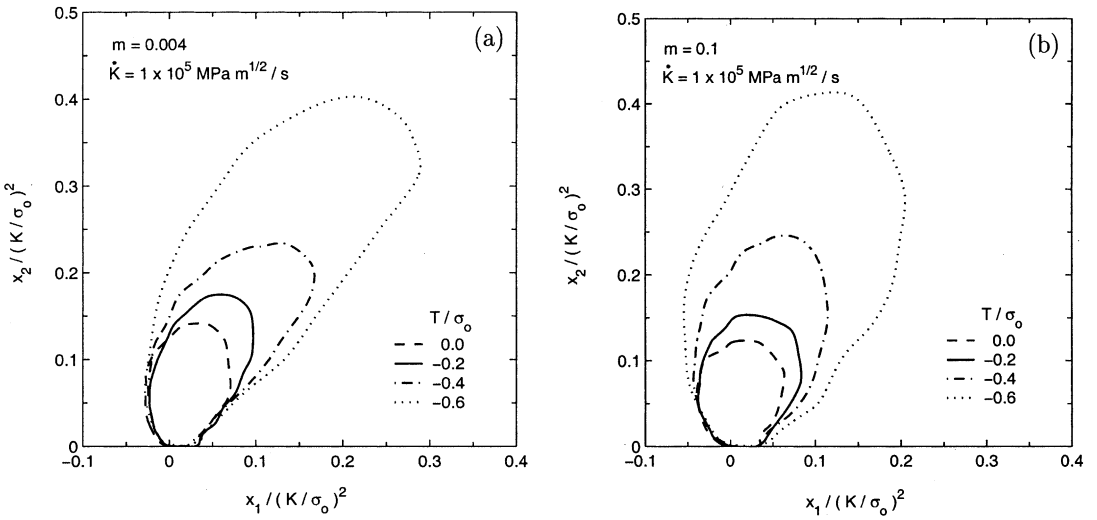

Fig. 7. Crack tip plastic zones obtained from the boundary layer analyses for different T-stress values corresponding to a fixed level of $\dot{K} = 10^5$ MPa $\sqrt{\text{m}}$/s for materials with (a) $m = 0.004$ and (b) $m = 0.1$. All results pertain to $K = 50$ MPa $\sqrt{\text{m}}$.

Table 2
Values of maximum plastic zone size obtained from the boundary layer analyses corresponding to two values of $\dot{K}$ and m for different T-stress values. All results pertain to $K = 50$ MPa $\sqrt{\text{m}}$

m	$\dot{K}$ (MPa $\sqrt{\text{m}}$/s)	T/σ_0	$(r_p)^{\max}/(K/\sigma_0)^2$
0.004	10^5	0	0.15
		−0.2	0.19
		−0.4	0.27
		−0.6	0.46
	10^7	0	0.15
		−0.2	0.19
		−0.4	0.27
		−0.6	0.45
0.1	10^5	0	0.13
		−0.2	0.17
		−0.4	0.25
		−0.6	0.43
	10^7	0	0.13
		−0.2	0.16
		−0.4	0.25
		−0.6	0.43

3. Analysis of SEN(T) specimen

In this section, quasi-static and dynamic elastic–viscoplastic finite element analyses of SEN(T) specimen are conducted. The dynamic analyses are performed for a range of loading rates. The stress distribution ahead of the crack tip and the plastic zone size and shape are systematically studied for different loading rates and strain rate sensitivity indices.

3.1. Modelling aspects

In Fig. 8, a schematic of the SEN(T) specimen, along with loads and boundary conditions are shown. The dimensions of the specimen are indicated in the figure. A crack length to width ratio $a/W = 0.5$ is considered. The quasi-static finite element analyses are performed by incrementing the load in small time steps such that the equilibrium solution is attained at each time step. Since the load versus time curves obtained from impact testing of fracture specimens generally exhibit a highly nonlinear variation (see, e.g., Zehnder et al., 1990), the applied load is chosen as a function of time t in the form $P(t) = \alpha t + \gamma t^2$ for the dynamic analyses. By varying the coefficients α and γ, a range of average stress intensity rates $\dot{K}$ from 10^5 to 2.5×10^6 MPa $\sqrt{\text{m}}$/s is achieved. The same load versus time functions, as well as coefficients α and γ, were used in the elastodynamic analyses conducted by Jayadevan et al. (2001a). This facilitates interpreting some of the results obtained from the present elastic–viscoplastic computations using the T-stress histories determined by Jayadevan et al. (2001a).

The viscoplastic constitutive model within the context of a small strain formulation described in Section 2 is employed to represent the material behaviour. The rate tangent modulus method proposed by Peirce et al. (1984) is used to update the stresses. Also, the material properties are taken to be the same as in Section 2, which correspond to a typical intermediate strength steel. In the dynamic analyses, the density ρ is chosen as 7800 kg/m^3 and the explicit central difference method (Zienkiewicz and Taylor, 1989) is employed to integrate the equations of motion. A small time step size (typically around 5×10^{-10} s), which is sufficient to

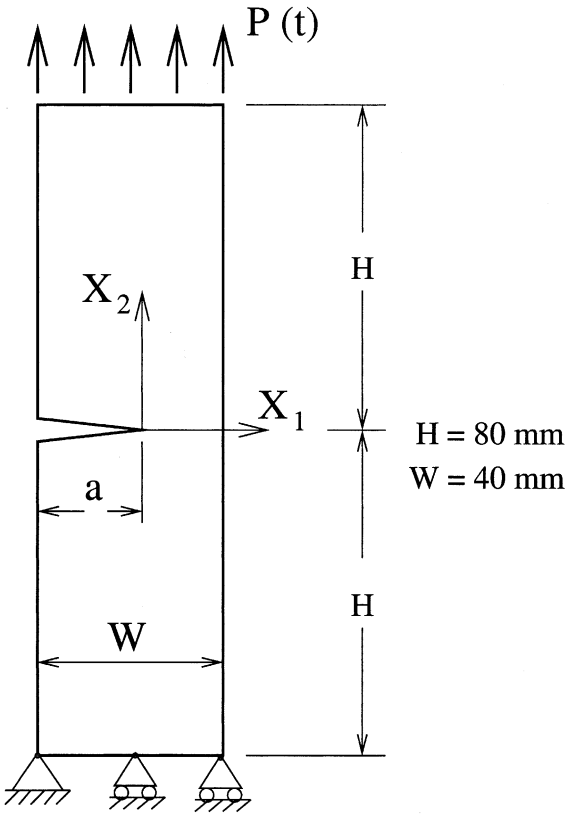

Fig. 8. Schematic of the SEN(T) specimen with $a/W = 0.5$.

ensure that the numerical solution remains stable, is used in these analyses. Also, the stability of the solution is continuously monitored by checking the global energy balance as suggested by Belytschko (1983) for nonlinear problems.

The domain integral method, proposed by Nakamura et al. (1986), is employed to compute the energy release rate from the finite element results. It must be mentioned that the above integral includes a term arising from inertial effects when applied to dynamic loading of a stationary crack (see, Nakamura et al., 1986). This term is neglected when quasi-static loading is considered. Several rectangular and circular domains are considered for estimating J and an average value of it is determined. Since the plastic zone is well contained in all the analyses carried out here, the stress intensity factor K is estimated from J as $K = \sqrt{EJ/(1-\nu^2)}$ (Freund, 1990). Further, the time histories of stress intensity factor obtained from the present analyses match closely with the corresponding histories computed by Jayadevan et al. (2001a) from their elastodynamic simulations. An average stress intensity rate $\dot{K}$ is computed from the stress intensity factor histories as

$$\dot{K} = \overline{K}/(\bar{t} - t_0), \tag{5}$$

where t_0 is the time taken for the longitudinal stress wave to arrive at the crack tip from the loading edge and $\bar{t}$ is the time required for K to attain a value of $\overline{K} = 50$ MPa $\sqrt{\text{m}}$. The value of $\bar{t}$ corresponding to each stress intensity rate $\dot{K}$ to be considered below can be deduced from the above equation, noting that $t_0 = 15.8$ μs for the chosen SEN(T) specimen.

The full geometry of the SEN(T) specimen (see Fig. 8) is modelled in the dynamic analyses since stress wave propagation effects render it as unsymmetric. The finite element mesh employed is composed of 1584 four-noded (2D plane strain) quadrilateral elements and 3342 degrees of freedom. It is well refined near the crack tip and is chosen based on a convergence study so that the evolution of important quantities, such as the J integral, as well as the stresses at finite distances ahead of the crack tip, are not affected by further refinement. The smallest element size near the tip is about 5 μm.

3.2. Results and discussion

3.2.1. Plastic zones

The crack tip plastic zones obtained from the dynamic analyses corresponding to different values of $\dot{K}$ are displayed in Fig. 9(a) and (b) for $m = 0.004$ and 0.1, respectively. Also plotted in these figures is the plastic zone from the rate independent static analysis at the same stress intensity factor of $K = 50$ MPa $\sqrt{\text{m}}$ (Jayadevan et al., 2001b) which is labelled as RI-static. Fig. 9(a) and (b) show that the plastic zone corresponding to $\dot{K} = 10^5$ MPa $\sqrt{\text{m}}$/s is quite close to that obtained from the rate independent static analysis. However, with increase in $\dot{K}$, the plastic zone rotates slightly clockwise and expands significantly in size. This feature is qualitatively similar to the rate independent case (Jayadevan et al., 2001b). Further, comparison of Fig. 9(b) with (a) shows that with increase in rate sensitivity index, the maximum extent of the plastic zone slightly reduces and it is less elongated in shape. Also, the plastic zone is more upright for higher m.

Here, it is recalled from the results presented in Section 2.2.4 that the shape and size of the plastic zone are not affected by the stress intensity rate under quasi-static loading at a given level of T-stress. However, it was found that with increase in negative T-stress the plastic zone enhances significantly in size. Thus, the effect of negative T-stress on the quasi-static plastic zone in Fig. 7 is akin to the influence of $\dot{K}$ on the plastic zone obtained from the dynamic analysis of the SEN(T) specimen as seen in Fig. 9. In order to clearly understand the above correlation, the value of T/σ_0 deduced from the elastodynamic analyses of Jayadevan et al. (2001a) corresponding to the same loading histories and stress intensity factor level ($K = 50$ MPa $\sqrt{\text{m}}$) as those considered in Fig. 9 are summarized in Table 3. Also presented in this table are the maximum plastic zone sizes determined from Fig. 9(a) and (b).

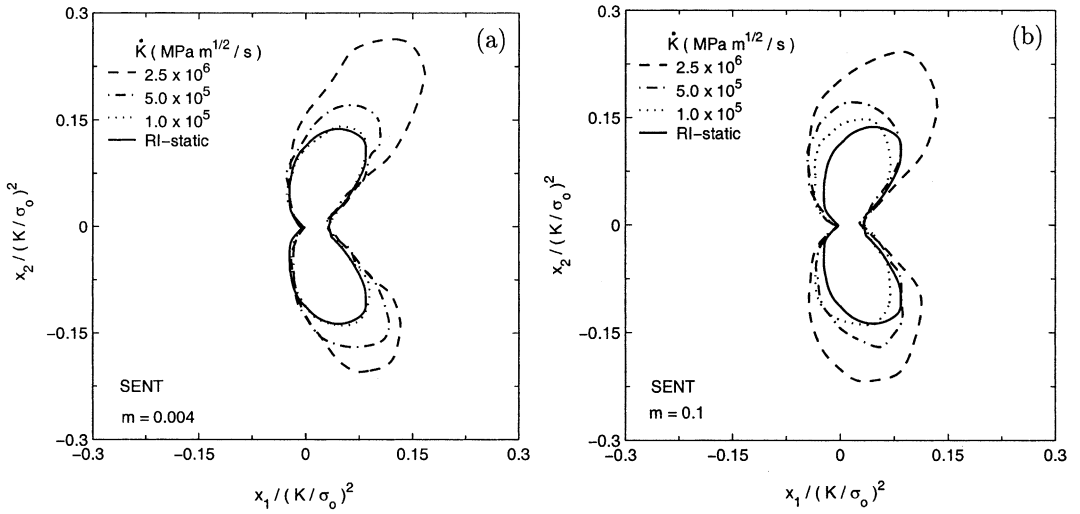

Fig. 9. Crack tip plastic zones for the specimen corresponding to different loading rates and $K = 50$ MPa $\sqrt{\text{m}}$ for (a) $m = 0.004$ and (b) $m = 0.1$. The corresponding plastic zone from the rate independent static analysis (Jayadevan et al., 2001b) is displayed as solid line.

It can be seen from Table 3 that the maximum plastic zone size increases with $\dot{K}$ irrespective of m. This is consistent with the fact that T/σ_0 obtained from the elastodynamic analysis is negative and increases in magnitude. Indeed, a comparison of the maximum plastic zone size presented in Table 3 with that corresponding to the same level of T/σ_0 determined from the quasi-static analysis which is given in Table 2 shows good agreement. Thus, the correlation between the influence of T-stress on the quasi-static plastic zone and the effect of $\dot{K}$ on the dynamic plastic zone is firmly established. Finally, a mild reduction in plastic zone size with increase in m can be observed from Table 3.

In order to illustrate the effect of material inertia, the crack tip plastic zones obtained from quasi-static and dynamic analysis of the SEN(T) specimen as well as from the small scale yielding analysis with $T = 0$ are shown in Fig. 10. They are labelled as SENT-QS, SENT-DYN and SSY, respectively. This figure pertains to $m = 0.1$ and $K = 50$ MPa $\sqrt{\text{m}}$. The quasi-static analysis of the SEN(T) specimen as well as the small scale yielding analysis were conducted using the same average $\dot{K} = 2.5 \times 10^6$ MPa $\sqrt{\text{m}}$/s as that observed in the dynamic analysis. It can be noticed that the plastic zones obtained from the above two quasi-static analyses are close to each other which is expected because T for the specimen is small in the limit of quasi-static loading as can be seen from Table 3. On the other hand, the plastic zone derived from

Table 3
Values of maximum plastic zone size from the dynamic analyses of the specimen at different loading rates for two values of m and corresponding to $K = 50$ MPa $\sqrt{\text{m}}$. Also indicated are the values of T/σ_0 for this specimen corresponding to the same loading histories and level of K deduced from the elastodynamic analyses of Jayadevan et al. (2001a)

m	$\dot{K}$ (MPa $\sqrt{\text{m}}$/s)	T/σ_0	$(r_p)^{\max}/(K/\sigma_0)^2$
0.004	1×10^5	−0.08	0.15
	5×10^5	−0.23	0.19
	2.5×10^6	−0.42	0.29
0.1	1×10^5	−0.08	0.15
	5×10^5	−0.23	0.18
	2.5×10^6	−0.42	0.26

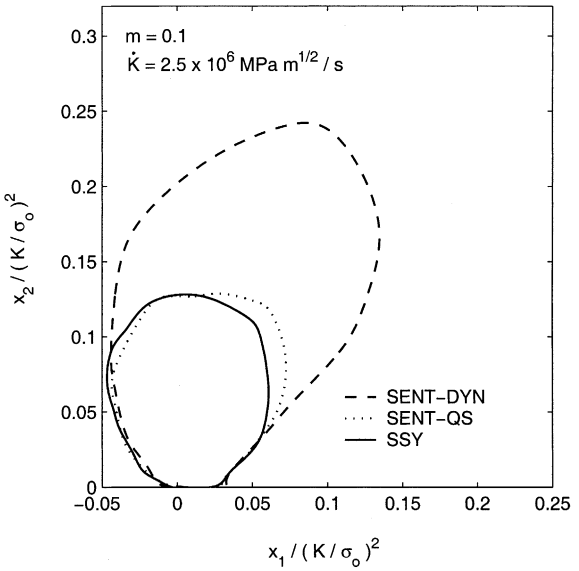

Fig. 10. A comparison of crack tip plastic zones obtained from dynamic and quasi-static analyses of the specimen as well as from the boundary layer model (with $T = 0$) corresponding to $K = 50$ MPa $\sqrt{\text{m}}$, $\dot{K} = 2.5 \times 10^6$ MPa $\sqrt{\text{m}}$/s and $m = 0.1$.

the dynamic analysis is much larger in size and rotated slightly clockwise owing to the large negative T at this $\dot{K}$ (see Table 3).

3.2.2. Stress distribution ahead of the crack tip

The radial variations of normalized opening stress obtained from the dynamic analyses of the SEN(T) specimen at different $\dot{K}$ corresponding to $m = 0.004$, 0.02 and 0.1 are displayed in Fig. 11(a)–(c), respectively. In addition, results from quasi-static analyses of the specimen corresponding to $\dot{K} = 10^4$ MPa $\sqrt{\text{m}}$/s are plotted in Fig. 11(b) and (c) and labelled as QS. Also shown in each figure for comparison is the stress variation obtained from static loading of the specimen with rate independent material properties (Jayadevan et al., 2001b).

On examining Fig. 11(a)–(c), it can be seen that the effect of $\dot{K}$ on the stress distribution ahead of the tip depends on the strain rate sensitivity index m. It should be recalled from Section 2.2.2 that strain rate sensitivity elevates the opening stress ahead of the crack tip as $\dot{K}$ increases at a given level of T when inertia is not taken into account. On the other hand, Jayadevan et al. (2001b) observed that for rate independent materials, the σ_{22} stress ahead of the crack tip obtained from dynamic analysis decreases significantly with increasing loading rate which is attributed to material inertia. Indeed, the constraint parameter Q becomes more negative for the rate independent case when $\dot{K}$ increases which correlates well with the development of large negative T-stress (see Table 3). The interplay of the above two opposing effects is expected to decide the actual stress variation ahead of the crack tip in dynamically loaded rate sensitive fracture specimens.

It may be seen from Fig. 11(a) that for $m = 0.004$, the stress variation corresponding to $\dot{K} = 10^5$ MPa $\sqrt{\text{m}}$/s is elevated slightly above the rate independent static case. However, with further increase in $\dot{K}$ it reduces, and falls well below the static variation. This behaviour is qualitatively similar to that observed by Jayadevan et al. (2001b) for a rate independent plastic material, although the reduction in the magnitude of σ_{22} at high loading rates in their work was more significant than that seen in Fig. 11(a).

Fig. 11(b) shows that strain rate effects for the case $m = 0.02$ are more pronounced than in Fig. 11(a) resulting in the stress variations corresponding to all $\dot{K}$ (including that from the quasi-static analysis) to be

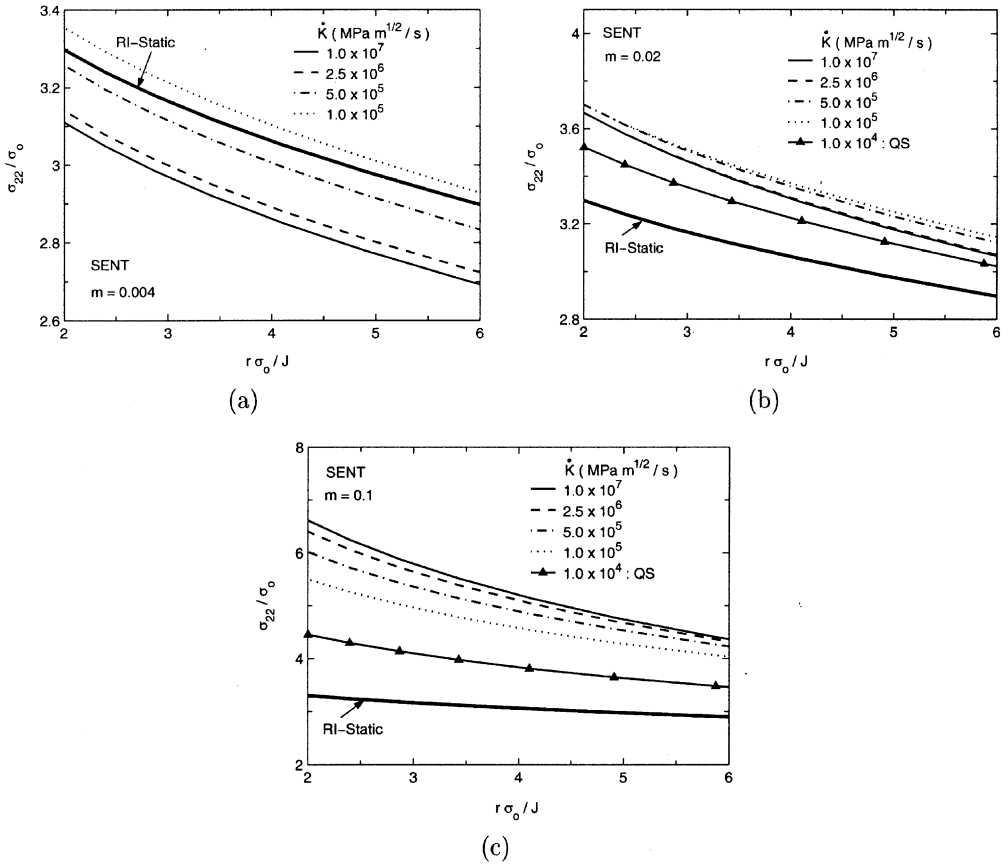

Fig. 11. The variation of normalized opening stress with radial distance ahead of the crack tip from the dynamic analyses of the specimen corresponding to $K = 50$ MPa $\sqrt{\text{m}}$ and different $\dot{K}$ for m values of (a) 0.004, (b) 0.02 and (c) 0.1. Similar results obtained from the quasi-static analysis at $\dot{K} = 10^4$ MPa $\sqrt{\text{m}}$/s and rate independent static analysis (Jayadevan et al., 2001b) of the specimen are also displayed.

elevated above the rate independent static curve. However, the opening stress at a given distance ahead of the tip decreases marginally when $\dot{K}$ exceeds 10^5 MPa $\sqrt{\text{m}}$/s which is caused by inertial effects. Thus, it may be inferred that for moderately high m like in Fig. 11(b), strain rate sensitivity dominates over material inertia up to $\dot{K} = 10^5$ MPa $\sqrt{\text{m}}$/s, whereas the reverse trend applies for higher $\dot{K}$ leading to slight reduction in the stress ahead of the tip.

By contrast, for a highly rate sensitive material (with $m = 0.1$), Fig. 11(c) shows that σ_{22} increases monotonically with $\dot{K}$. The opening stress obtained from the quasi-static analysis with $\dot{K} = 10^4$ MPa $\sqrt{\text{m}}$/s is about 25% higher than the rate independent static limit at $r\sigma_0/J = 4$, and falls below those from dynamic analyses. However, the enhancement in σ_{22} with $\dot{K}$ is marginal at high values of $\dot{K}$. It is found that while σ_{22} pertaining to $\dot{K} = 10^5$ MPa $\sqrt{\text{m}}$/s in Fig. 11(c) is slightly higher than the corresponding quasi-static variation given in Fig. 3(b), it falls below the latter at $\dot{K} = 10^7$ MPa $\sqrt{\text{m}}$/s. However, the plastic strain rate ahead of the tip computed from the dynamic analysis is much higher than that given in the quasi-static simulation at the same $\dot{K}$. Hence, strain rate sensitivity and inertial effects are inherently coupled in Fig. 11(c). A quasi-static reference field which accounts for flow stress elevation at the same strain rate ahead of the tip as obtained in the dynamic analysis is needed for the purpose of quantifying inertia-driven constraint

loss. To this end, a modification to the HRR solution taking into account the current flow stress was suggested by Basu and Narasimhan (2000), but this approach is not pursued here because it is ad-hoc in nature.

The opposing roles of strain rate sensitivity and material inertia as discussed above is also expected to reflect in the variation of cleavage fracture toughness with loading rate.

4. Variation of dynamic fracture toughness with loading rate

In this section, the variations of dynamic fracture toughness K_{dc} associated with cleavage crack initiation versus stress intensity rate $\dot{K}$, predicted by the numerical results, are presented. To this end, the simple critical stress criterion proposed by Ritchie et al. (1973) is employed. This criterion requires that the opening stress σ_{22} should exceed a critical value σ_c over a characteristic distance r_c ahead of the tip. The time history of stress at the critical distance r_c (say, for example, 75 μm) ahead of the tip, computed from the finite element analysis, for each loading case is examined. From this history, the time and, hence, the value of stress intensity factor at which σ_{22} attains the critical level σ_c (say, for example, $3\sigma_0$) is deduced. Thus, the dynamic fracture toughness predicted by the analysis for each loading case is determined. In order to simplify the computational effort, the fracture toughness for $\dot{K} < 10^4$ MPa $\sqrt{\text{m}}$/s are obtained using quasi-static analysis, since inertial effects are expected to be negligible.

The variation of K_{dc} with $\dot{K}$ for different values of m predicted using $r_c = 75$ and 125 μm are shown in Fig. 12(a) and (b), respectively. The value of σ_c is assumed as $3\sigma_0$ in these figures. Also presented in this figure is the variation of K_{dc} with $\dot{K}$ deduced from the rate independent analysis (labelled as RI) performed by Jayadevan et al. (2001b). For this case, K_{dc} is almost constant at the static fracture toughness value up to $\dot{K} = 10^5$ MPa $\sqrt{\text{m}}$/s and thereafter, increases steeply. This is attributed to the decrease in opening stress or enhanced constraint loss at high $\dot{K}$ for rate independent plastic materials which is caused by material inertia. The curve pertaining to $m = 0.004$ is similar to the rate independent case, except that it shows a marginal decrease in K_{dc} between $\dot{K} = 10^3$–10^5 MPa $\sqrt{\text{m}}$/s. However, a local minimum in K_{dc} occurs at $\dot{K} \approx 10^5$ MPa $\sqrt{\text{m}}$/s, and it increases steeply with further elevation in $\dot{K}$ like the rate independent case. The slightly decreasing branch in the K_{dc}–$\dot{K}$ curve is caused by strain rate sensitivity which tends to elevate the stress

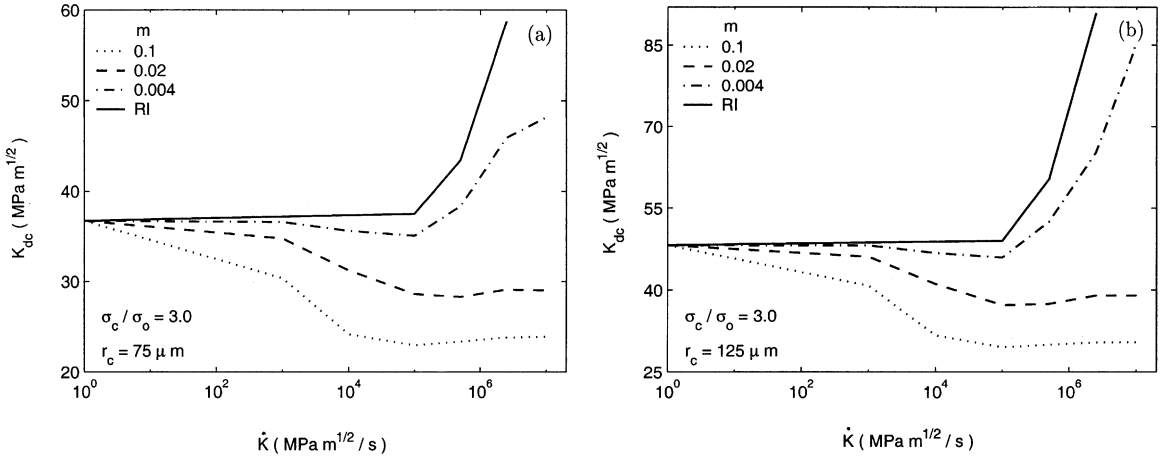

Fig. 12. The variation of dynamic fracture toughness K_{dc} with loading rate $\dot{K}$ corresponding to $\sigma_c/\sigma_0 = 3.0$ and r_c of (a) 75 and (b) 125 μm for the specimen with different rate sensitivity indices. Similar results corresponding to the rate independent case (Jayadevan et al., 2001b) are displayed as solid lines.

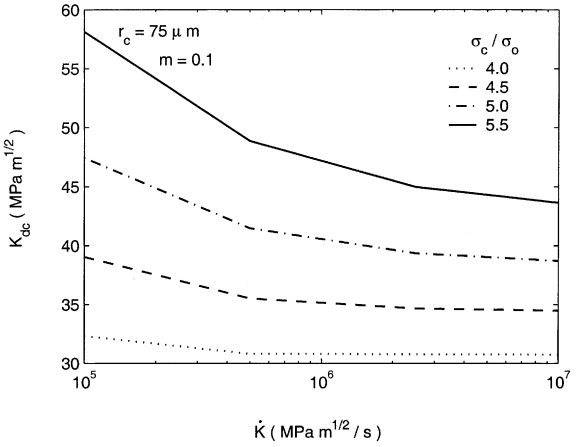

Fig. 13. The variation of dynamic fracture toughness K_{dc} at high loading rates corresponding to $r_c = 75$ μm and different values of σ_c/σ_0 for the specimen with $m = 0.1$.

ahead of the tip up to $\dot{K} = 10^5$ MPa $\sqrt{\text{m}}$/s as seen in Fig. 11(a). As the rate sensitivity index m increases, the reduction in K_{dc} up to an intermediate level of $\dot{K}$ becomes more pronounced owing to the strong elevation in stress (see Fig. 11(b), (c)). This is qualitatively similar to experimental observations (see, for example, Costin and Duffy (1979) or Kalthoff (1986)). On the other hand, as noted in connection with Fig. 11(b) and (c), material inertia retards further elevation in stress for $\dot{K} > 10^5$ MPa $\sqrt{\text{m}}$/s. This halts the reduction in K_{dc} and leads to the K_{dc}–$\dot{K}$ curve attaining a plateau for $m = 0.02$ and 0.1 in Fig. 12(a) and (b). Finally, on comparing Fig. 12(a) and (b) it can be seen that K_{dc} increases when the critical distance r_c is increased.

The effect of critical stress ratio σ_c/σ_0 on the K_{dc}–$\dot{K}$ variation at high loading rates (in the range from 10^5 to 10^7 MPa $\sqrt{\text{m}}$/s) is displayed in Fig. 13. These K_{dc}–$\dot{K}$ curves correspond to $m = 0.1$ and $r_c = 75$ μm. It may be seen from Fig. 13 that for high values of σ_c/σ_0, the dynamic fracture toughness continues to decrease with $\dot{K}$ (but at a diminishing rate) up to 10^7 MPa $\sqrt{\text{m}}$/s. On the other hand, this effect is less pronounced for low values of σ_c/σ_0 which results in the plateau region seen in Fig. 12.

5. Conclusions

The main conclusions of this work are summarized as follows:

1. Quasi-static boundary layer analyses show that the near-tip fields when plotted against $r\sigma_0/J$ are parametrized by $\dot{K}/(K\dot{\varepsilon}_0)$ for any given T. The loading rate significantly elevates the opening stress ahead of the crack tip at any given level of T and K, for highly rate sensitive materials. On the other hand, normalized crack tip plastic zones are unaffected by loading rate when inertia is not accounted. However, a marginal effect of the rate sensitivity index on the plastic zones is observed.
2. The boundary layer analyses show that a two-parameter (J–Q) characterization of crack tip fields is valid in low to moderately rate sensitive materials. Thus, the difference field (Q-term) with respect to the reference ($T = 0$) solution becomes strongly negative as T-stress increases in the negative direction. Also, it is slowly varying with respect to distance ahead of the tip and is triaxial in nature. These latter features break down for a highly rate sensitive material (like $m = 0.1$). An imposition of negative T-stress causes a slight clockwise rotation of the plastic zone and significant enhancement in size as in rate independent plastic solids.

3. An inertia-driven constraint loss at high $\dot{K}$ in a dynamically loaded fracture specimen is observed for materials with low m. However, for high values of m, this is not clearly apparent from the stress distribution ahead of the crack tip since rate sensitivity and inertial effects are inherently coupled. Further, since a quasi-static reference field which accounts for flow stress elevation at the same level of strain rate ahead of the tip as obtained in the dynamic analysis is not available, it is not possible to quantify inertia-driven constraint loss in highly rate sensitive materials. On the other hand, the plastic zones obtained from the dynamic analyses show significant enhancement in size at high $\dot{K}$ and correlate well with those from quasi-static analyses at the same level of (negative) T-stress.
4. The dynamic fracture toughness K_{dc} associated with cleavage crack initiation decreases with $\dot{K}$ for rate sensitive materials which agrees with experimental observations. However, a local minimum occurs at $\dot{K} \approx 10^5$ MPa $\sqrt{\text{m}}$/s for $m = 0.004$ which is followed by a steep elevation in K_{dc} similar to the rate independent case. The materials with higher m display a plateau in the variation of K_{dc} with $\dot{K}$ above a certain loading rate. Thus, the nature of the K_{dc}–$\dot{K}$ variation depends critically on the rate sensitivity index of the material.

References

Al-Ani, A.M., Hancock, J.W., 1991. *J*-dominance of short cracks in tension and bending. Journal of the Mechanics and Physics of Solids 39, 23–43.

Basu, S., Narasimhan, R., 2000. A numerical investigation of loss of crack tip constraint in a dynamically loaded ductile specimen. Journal of the Mechanics and Physics of Solids 48, 1967–1985.

Belytschko, T., 1983. An overview of semi-discretization and time integration procedures. In: Belytschko, T., Hughes, T.J.R. (Eds.), Computational Methods for Transient analysis. Elsevier, Amsterdam.

Betegón, C., Hancock, J.W., 1991. Two-parameter characterization of elastic–plastic crack-tip fields. Transactions of the ASME, Journal of Applied Mechanics 58, 104–110.

Costin, L.S., Duffy, J., 1979. The effect of loading rate and temperature on the initiation of fracture in a mild, rate-sensitive steel. Transactions of the ASME, Journal of Engineering Materials and Technology 101, 258–264.

Dally, J.W., Barker, D.B., 1988. Dynamic measurements of initiation toughness at high loading rates. Experimental Mechanics 28, 298–303.

Freund, L.B., 1990. Dynamic Fracture Mechanics. Cambridge University Press, Cambridge.

Hoff, R., Rubin, C.A., Hahn, G.T., 1985. Strain-rate dependence of the deformation at the tip of a stationary crack. ASTM STP 868, pp. 409–430.

Hughes, T.J.R., 1980. Generalization of selective integration procedures to anisotropic and non-linear media. International Journal of Numerical Methods in Engineering 15, 1413–1418.

Hutchinson, J.W., 1968. Singular behaviour at the end of a tensile crack in a hardening material. Journal of the Mechanics and Physics of Solids 16, 13–31.

Jayadevan, K.R., Narasimhan, R., Ramamurthy, T.S., Dattaguru, B., 2001a. A numerical study of T-stress in dynamically loaded fracture specimens. International Journal of Solids and Structures 38, 4987–5005.

Jayadevan, K.R., Narasimhan, R., Ramamurthy, T.S., Dattaguru, B., 2001b. Constraint loss under dynamic loading in rate independent plastic solids. International Journal of Fracture, submitted for publication.

Kalthoff, J.F., 1986. Fracture behaviour under high rates of loading. Engineering Fracture Mechanics 23, 289–298.

Kanninen, M.F., O'Donoghue, P.E., 1995. Research challenges arising from current and potential applications of dynamic fracture mechanics to the integrity of engineering structures. International Journal of Solids and Structures 32, 2423–2445.

Klepaczko, J.R., 1982. Discussion of a new experimental method in measuring fracture toughness initiation at high loading rates by stress waves. Transactions of the ASME, Journal of Engineering Materials and Technology 104, 29–35.

Koppenhoefer, K.C., Dodds Jr., R.H., 1996. Constraint effects on fracture toughness of impact-loaded, precracked Charpy specimens. Nuclear Engineering and Design 162, 145–158.

Liu, C., Knauss, W.G., Rosakis, A.J., 1998. Loading rates and the dynamic initiation toughness in brittle solids. International Journal of Fracture 90, 103–118.

Nakamura, T., Shih, C.F., Freund, L.B., 1986. Analysis of a dynamically loaded three-point-bend ductile fracture specimen. Engineering Fracture Mechanics 25, 323–339.

O'Dowd, N.P., Shih, C.F., 1991. Family of crack-tip fields characterized by a triaxiality parameter—I. Structure of fields. Journal of the Mechanics and Physics of Solids 39, 989–1015.

O'Dowd, N.P., Shih, C.F., 1992. Family of crack-tip fields characterized by a triaxiality parameter—II. Fracture applications. Journal of the Mechanics and Physics of Solids 40, 939–963.

O'Dowd, N.P., Shih, C.F., 1994. Two-parameter fracture mechanics: Theory and applications. ASTM STP 1207, pp. 21–47.

Owen, D.M., Zhuang, S., Rosakis, A.J., Ravichandran, G., 1998a. Experimental determination of dynamic crack initiation and propagation fracture toughness in thin aluminum sheets. International Journal of Fracture 90, 153–174.

Owen, D.M., Rosakis, A.J., Johnson, W.L., 1998b. Dynamic failure mechanisms in beryllium-bearing bulk metallic glasses. SM Report 98-22, GALCIT, California Institute of Technology, Pasadena, USA.

Peirce, D., Shih, C.F., Needleman, A., 1984. A tangent modulus method for rate dependent solids. Computers and Structures 18, 875–887.

Priest, A.H., 1976. Influence of strain rate and temperature on the fracture and tensile properties of several metallic materials. Proceedings of the International Conference on Dynamic Fracture Toughness, Welding Institute, Cambridge, pp. 95–111.

Ravi-Chandar, K., Knauss, W.G., 1984. An experimental investigation into dynamic fracture: I. Crack initiation and arrest. International Journal of Fracture 25, 247–262.

Rice, J.R., Rosengren, G.F., 1968. Plane strain deformation near a crack tip in a power-law hardening material. Journal of the Mechanics and Physics of Solids 16, 1–12.

Ritchie, R.O., Knott, J.F., Rice, J.R., 1973. On the relationship between critical tensile stress and fracture toughness in mild steel. Journal of the Mechanics and Physics of Solids 21, 395–410.

Rosakis, A.J., Ravichandran, G., 2000. Dynamic failure mechanics. International Journal of Solids and Structures 37, 331–348.

Shih, C.F., O'Dowd, N.P., Kirk, M.T., 1993. A framework for quantifying crack tip constraint. ASTM STP 1171, pp. 2–20.

Venkert, A., Guduru, P.R., Ravichandran, G., 1998. Mechanisms of dynamic failure in Ni–Cr steels. SM Report 98-5, GALCIT, California Institute of Technology, Pasadena, USA.

Williams, M.L., 1957. On the stress distribution at the base of a stationary crack. Transactions of ASME, Journal of Applied Mechanics 24, 109–114.

Zehnder, A.T., Rosakis, A.J., 1990. Dynamic fracture initiation and propagation in 4340 steel under impact loading. International Journal of Fracture 43, 271–285.

Zehnder, A.T., Rosakis, A.J., Krishnaswamy, S., 1990. Dynamic measurement of the *J*-integral in ductile metals: comparison of experimental and numerical techniques. International Journal of Fracture 42, 209–230.

Zienkiewicz,, O.C., Taylor, R.L., 1989. The finite element method, fourth ed. Solid and Fluid Mechanics, Dynamics and Non-linearity, vol. 2. McGraw-Hill, UK.